AGU
ADVANCING
EARTH AND
SPACE SCIENCE

Geophysical Research Letters

Broadband Infrasound Signal of a Collapsing Hanging Glacier

Emanuele Marchetti[1] , Fabian Walter[2], and Lorenz Meier[3]

[1]Department of Earth Sciences, University of Firenze, Firenze, Italy, [2]Laboratory of Hydraulics, Hydrology and Glaciology VAW, ETH Zürich, Zürich, Switzerland, [3]Geopraevent AG, Zürich, Switzerland

Abstract A major ice collapse ($\approx$10,000 m^3) from a hanging glacier on Mount Eiger, Switzerland was recorded by a small aperture array as a broadband (0.1–10 Hz) infrasound signal. Array analysis reveals that the high ($\approx$3 Hz) frequency signal is infrasound produced by the moving ice mass, and its back azimuth variation with time tracks the ice mass trajectory and provides a mean velocity estimate. Infrasound frequency is used to estimate a radius, that despite overestimating the volume, provides quantitative analysis in near-real time. The low ($\approx$0.1 Hz) frequency oscillation is modeled in terms of the velocity field (wind), which the moving ice mass induces on the surrounding air, producing pressure variations at the different elements. These results show how infrasound array observations may provide quantitative information of glacier collapse and ice avalanche trajectories, and possibly, volume.

Plain Language Summary Ice avalanches constitute severe natural hazards, threating human lives and infrastructures, and are expected to increase with ongoing climate change and population pressure forcing settlements into exposed terrain. In Europe, costly monitoring programs have also highlighted changing glacial hazards. Consequently, monitoring and warning systems, which help mitigate the threat and impact of mass movements are a key component of hazard management in mountainous regions worldwide. In this study we show how a major ice collapse ($\approx$10,000 m^3) from a hanging glacier on Mount Eiger, Switzerland, was recorded with an infrasound (low frequency sound) monitoring system and how it allowed to evaluate the volume, trajectory and velocity of the falling ice mass. Moreover, thanks to a detailed analysis the broad (0.1–10 Hz) frequency component of the signal, the ice avalanche was fully investigated and modeled in terms of the fluid dynamics of the falling mass. These results show how infrasound array observations may provide quantitative information of glacier collapse and ice avalanche volume, thus opening new perspectives for monitoring avalanching glaciers and providing warning for break-off events.

1. Introduction

Rapid alpine mass movements such as ice or rock avalanches, rock falls and debris flows constitute severe natural hazards. They threaten human lives and infrastructure and are expected to increase with ongoing climate change and population pressure forcing settlements into exposed terrain (Field et al., 2014). Recently, glacier collapses have caught particular attention of scientists and stakeholders. The twin collapses of two Tibetan glaciers in 2017 were a sudden reminder that climate change may produce glacial hazards in new places and with unexpected dimension (Kääb et al., 2018). In Europe, costly monitoring programs have also highlighted changing glacial hazards: Glacial retreat produces new and potentially unstable ice geometries, and warming atmosphere and mountain faces change the thermal regime of already unstable ice (Faillettaz et al., 2015; Faillettaz, Sornette, & Funk, 2011; Preiswerk et al., 2016; Raymond et al., 2016). The latter mechanism implies that hitherto cold based ice cover frozen to steep mountain faces ("hanging glaciers") may warm towards a temperate basal regime leading to sliding instabilities (Preiswerk et al., 2016). With most unstable ice collapses happening unnoticed, the number of well documented events is small, which complicates systematic studies of break-off activity in relation to climatic factors. Instead, successful early warning still relies on experienced observers identifying unstable ice and subsequent monitoring.

Several studies showed that major events are typically preceded by an acceleration of the ice surface that can be used to predict the timing of the break-off (Faillettaz et al., 2015). High resolution photogrammetry and ground based interferometry (GBInSAR) (Meier et al., 2016) reliably capture such acceleration, albeit at the

cost of sophisticated and expensive instrument deployment, targeting only a small and predefined glacier region. In search of more affordable monitoring methods, researchers have turned to seismic techniques, which detect ground unrest in response to ice failure, avalanche propagation and even precursory englacial damage growth (Dalban Canassy et al., 2012, 2013; Faillettaz et al., 2015; Faillettaz, Funk, & Sornette, 2011; Pralong et al., 2003). Unfortunately, microseismicity near glaciers tends to mask signals related to ice break-off and to date volumes of unstable or detaching ice seracs cannot be estimated from seismic data alone.

Analogous to seismic waves, mass movements induce acoustic waves in the atmosphere, which can be recorded in the infrasonic range typically taken as frequencies below 20 Hz. Snow avalanches (Naugol-nykh & Bedard, 1990), rockfalls (Johnson & Ronan, 2015) and debris flows (Allstadt et al., 2018; Marchetti et al., 2019) have thus been studied with infrasound measurements. Although infrasound sensors are not sensitive to the acceleration of the ice surface preceding major events, as a fast perturbation of the atmosphere is required to radiate infrasound acoustic waves, rapid event detection for hazard mitigation is in principle possible. For example, infrasound detections could be used to monitor snow avalanches and debris flows in order to alert people in affected terrain and trigger road closures (Marchetti et al., 2015, 2019; Schimmel et al., 2018).

So far, relatively little research has focused on infrasound monitoring of glacier break-off events and resulting ice avalanches. With the help of standard array methods, even weak and distant infrasound recordings can detect and locate ice break-off events (Preiswerk et al., 2016). Continuous monitoring, and detection, of break-off events might allow to identify periods of increased instability, and therefore potentially lead to a risk mitigation. However, it is not clear which other types of information are contained in the infrasound signature of glacier break-off events and resulting ice avalanches, possibly relating to event size and/or dynamics.

In this study we present an infrasound analysis of a break-off from the hanging glacier at Mount Eiger, Switzerland. We show that the infrasound signature is broadband containing low-frequency (0.1 Hz) pressure oscillations in addition to signals around 3 Hz, which are of the kind that has been used in previous mass movement studies. We model the low-frequency signals as pressure variations, induced by the flow of air around the moving avalanche mass. The combination of the various signal components provides constraints on ice avalanche location, trajectory, velocity and volume.

2. Hanging Glacier on Mount Eiger, Switzerland

The hanging glacier is located at an elevation of around 3,400 m above sea level on the west face of Mount Eiger in the Swiss Alps. The glacier is partly frozen to its bedrock with the presence of temperate zones (Faillettaz et al., 2015; Margreth et al., 2017). Located above steep slopes, the glacier produces periodic break-off events in form of ice serac collapses from the 200 m wide and 30 m tick front, leading to ice avalanches that are typically <10,000 m^3 (Margreth et al., 2017). The collapses are driven by gravity and occur upon significant englacial damage growth at a point when the ice can no longer sustain its weight (Faillettaz et al., 2015). Glacier front stability is controlled mostly by an average ice velocity at the glacier front of 7 m/y producing a yearly ice flux of 40,000 m^3 through the frontal flux gate whose area is 6,000 m^2 (Margreth et al., 2017).

Given negligible surface melt, collapse events balance the ice flux, resulting in ice release events with volumes ranging between 1,000 and 100,000 m^3. An ice collapse of 100,000 m^3 occurred on August 20, 1990 (Pralong & Funk, 2006). If the basal thermal regime of the hanging glacier changes in response to bedrock warming and latent heat transfer, break-off failures significantly larger that 100,000 m^3 (Margreth et al., 2017) may occur without any clear precursor events (Faillettaz, Sornette, & Funk, 2011).

Ice avalanches detaching from the hanging glacier front travel over 400 m through a steep gully before entering a wider area covered with snow and ice debris produced by avalanches and previous ice collapses. Depending on this pre-existing snow cover, entrainment may enhance runout and the destructive potential of break-off events. At lower elevations, the rocky Rotstock Ridge emerges 55–110 m above its surrounding terrain, breaking and deflecting the avalanche flow southwest. This counter clockwise deflection of the flow
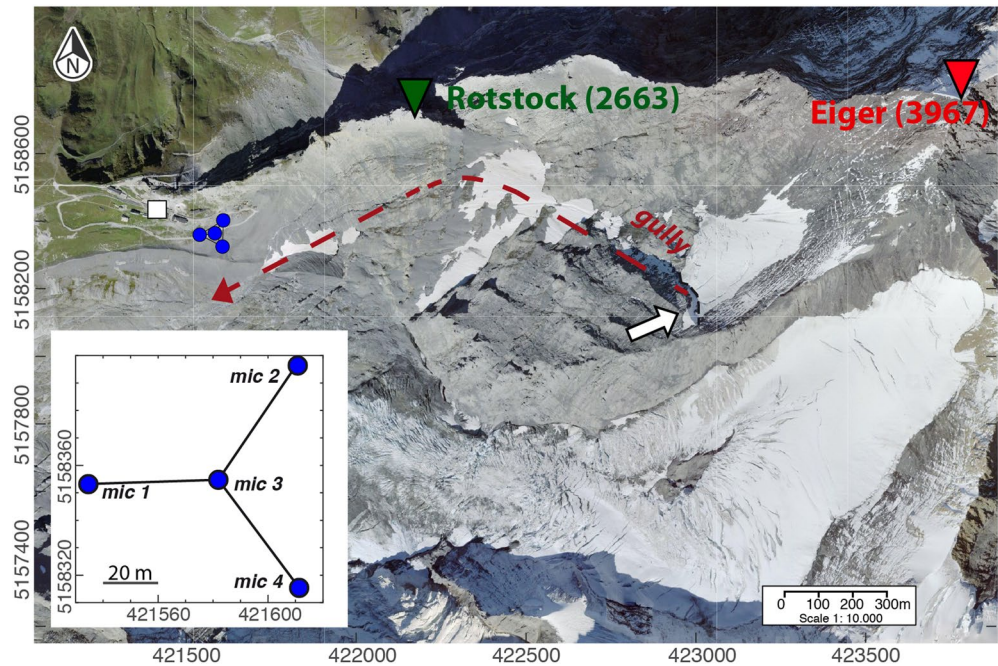
Figure 1. Location of the infrasound array (blue dots), positioned nearby the Eigergletscher train station (white square), and of the avalanching front (white arrow) of the hanging glacier on Mount Eiger. The location of Mount Eiger (reversed red triangle) and the Rotstock Ridge (reversed green triangle) peaks is marked for reference. Detached ice lamellas typically flow within a narrow gully before being deflated anti-clockwise by the Rotstock Ridge (red dashed arrow). The geometry of the four elements of the array is shown in the inlet. Spot image reproduced by ©/with permission/2020 swisstopo (JD100042).

to some extent shields the Eigergletscher train station (Figure 1). However, the train station is likely exposed to larger events that include substantial entrainment of powder snow (Margreth et al., 2017).

3. Instrumentation and Data

An infrasound array was deployed at an elevation of ≈2,300 m, near the station Eigergletscher of the Jungfraujoch Railway (Figure 1). The main front of the hanging glacier locates ≈1.4 km East of and 900 m above the array.

The infrasound array was equipped with four PRS0100a pressure sensors by Item s.r.l., with a sensitivity of 25 mV/Pa in the pressure range of ±100 Pa and frequency response between 0.02 and 100 Hz. The four sensors of the array were deployed with a triangular geometry (Figure 1), three sensors deployed at the vertices and one sensor deployed at the center and co-located with 4-channel digitizer (Guralp CMG/DM24). Maximum distance between two elements of the array was ≈60 m. Infrasound data provided by each array element were digitized at 24 bits and 100 Hz, GPS time stamped, recorded locally and made available through TCP/IP with a 3G modem. The pressure sensors were installed in plastic containers that were buried in the ground and covered with stones to reduce wind noise and increase the signal-to-noise ratio. Near the infrasound array, an interferometric radar was installed to predict break-off events via detection of unusual ice front velocities (Margreth et al., 2017).

4. Serac Collapse on 29 May 2017

In the early morning of May 29, 2017, a substantial serac collapse occurred from the hanging glacier (Figure 2). The collapse was preceded by an acceleration of parts of the ice front to nearly 200 mm per day. The radar image calculated between 01:00 and 07:00 UT showed that the unstable serac covered an area about 10% larger than the equivalent 200 m^2 surface area of the April 12, 2016 break-off documented in Margreth
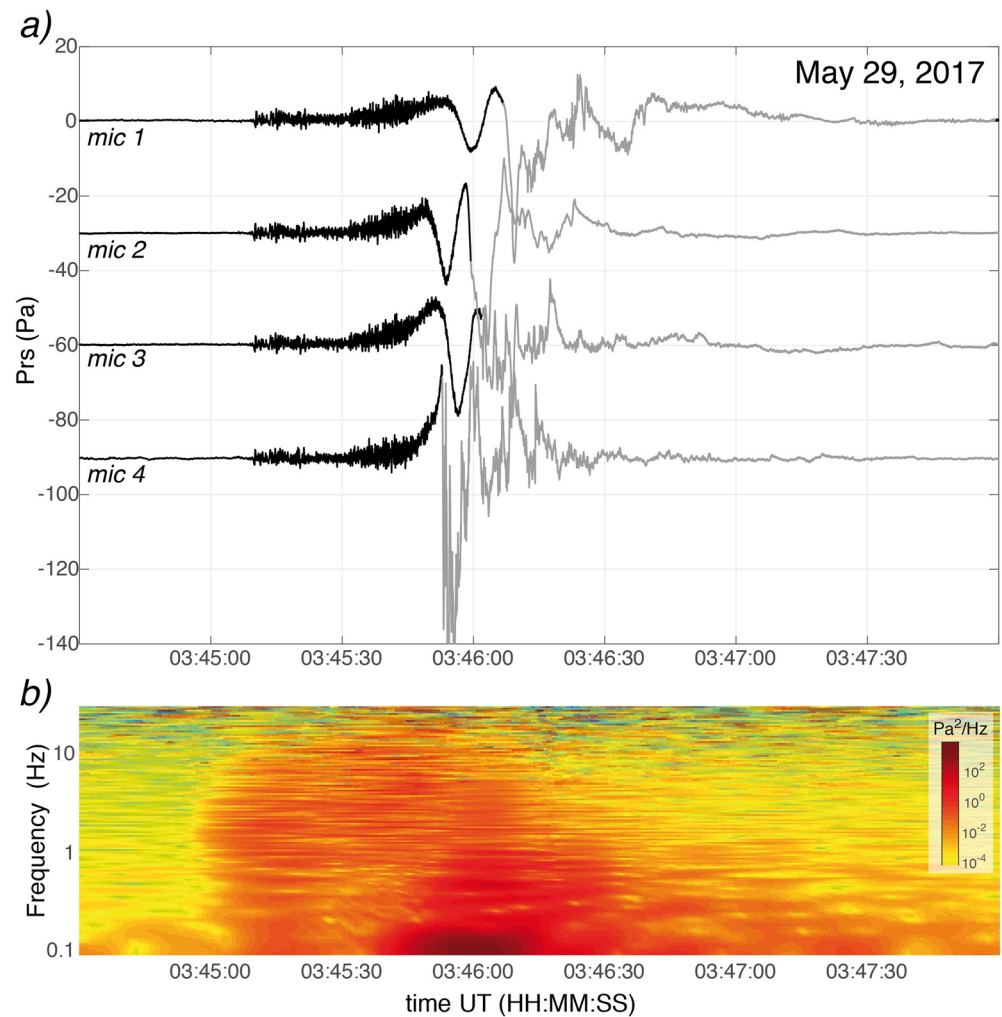
Figure 2. (a) Infrasonic record of the collapse at the 4 elements of the array. The signal is colored in gray once the spurious phase is recorded. (b) Spectrogram of the signal recorded by sensor 2 showing a main peak around 0.1 Hz preceded by a higher frequency (3 Hz) phase.

et al. (2017) (Supporting Information S1). Assuming that pervasive crevasses leading to serac separation develop 40–50 m behind the ice front (Pralong et al., 2003) yields a volume estimate of 8,800–11,000 m³.

The collapsing serac fell nearly vertically for ≈600 m within the east-west gully and eventually the trajectory turned from NW to SW behind Rotstock Ridge before it continued moving downhill in a more or less straight line (red dashed line in Figure 1). The powder cloud reached the buildings of the Eigergletscher train station next to the infrasound antenna and material partly covered the infrasound array. Sensor four (Figure 1, inlet), in particular, was covered by snow and ice blocks.

The event was clearly recorded by the infrasound array at 03:45:10 UT, as a long-lasting (≈150 s), large amplitude (>70 Pa peak-to-peak), broadband signal (Figure 2). The timing (this was the only infrasound signal in the period identified by the radar) and wave parameters discussed in Section 5 allows us to unambiguously relate the recorded infrasound signal to the collapse. Higher frequency signals, peaking around 2.5–3 Hz, extend to well above 10 Hz. These signals are super-imposed on a low-frequency oscillation, peaking around 0.1 Hz (Figure 2b).

The high frequency energy is most visible during the fist part of the signal, until 03:45:55. The low frequency signal starts as a smooth pressure increase around 03:45:35, ≈25 s after the high frequency signal onset was recorded at the array and within a few seconds it begins to dominate the entire spectrum. The low frequency
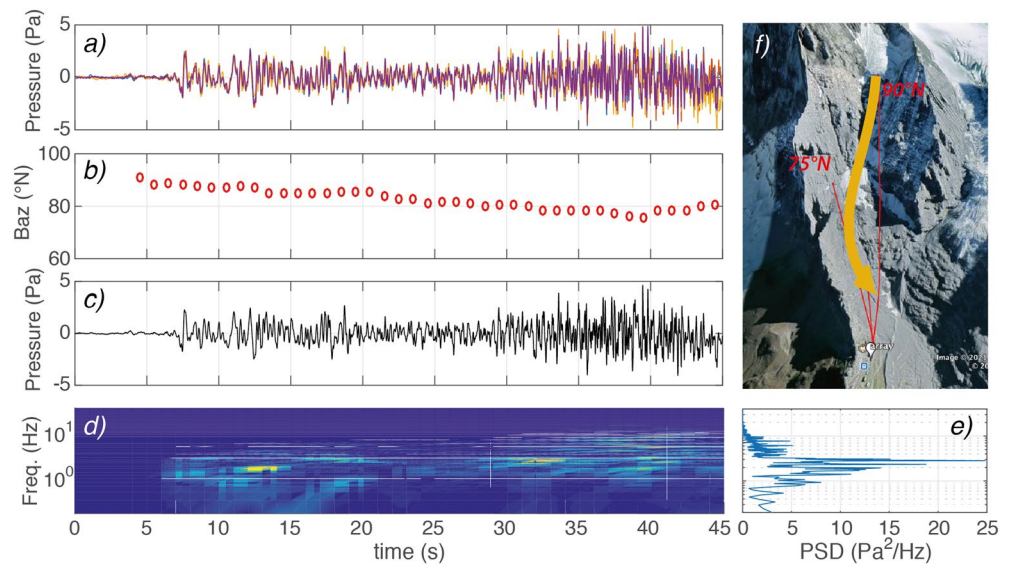
Figure 3. Amplitude (Pa at the array) of the recorded signal band-pass filtered between 0.1 and 25 Hz, (a). Back azimuth (b) of infrasound detections. (c) Stacked waveform along the beam and (d) corresponding PSD spectrogram and (e) amplitude. Timing is expressed as seconds after 3:45 UTC. (f) GoogleEarth projection of back azimuth values of 90, 75 and 82° N (red lines) constraining the possible avalanche path (orange arrow).

oscillations reach a first positive peak of ≈10–15 Pa, within 18–23 s of their onset (Figure 2a). This low frequency oscillation is showing a different frequency content at the different elements of the array. Peak frequency, measured as the inverse of the time difference between the two positive peaks, decreases from 0.11 Hz (9 s time difference) for mic 2, down to 0.085 Hz (11.6 s time difference) for mic 1. Moreover, the low frequency signal is marked by large time delays at the different array elements (≈6 s between mic 1 and mic 2 and ≈2.5 s between mic 2 and mic 3), with the signal first recorded at sensor 2. Considering the small aperture (≈60 m) of the array, these delays are consistent with a propagation velocity of a few tens of m/s, well below the propagation velocity of sound.

The waveforms show a third spurious phase (gray in Figure 2). The timing of this phase varies across the array. It is first recorded at 03:45:52 UT, before the first positive peak of the low frequency oscillation was reached, at sensor 4, end eventually, 15 s afterwards at 03:46:07 UT, at sensor 1. This spurious phase might be produced by snow and/or small ice debris depositing on the sensors.

5. Array Analysis of High-Frequency (3 Hz) Signals

In order to interpret the initial, high-frequency (3 Hz) infrasonic signal generated as the ice avalanche approaches the antenna, we perform coherence analysis of infrasound data recorded at the 4 array elements (Figure 3a). We apply cross-correlation analysis in discrete time windows of 5 s with 4 s overlap to 1–10 Hz band-pass filtered infrasound data. Once coherent signals are observed throughout the array, we evaluate time delays among the array elements following Ulivieri et al. (2011). This gives the propagation back azimuth (Figure 3b) of the infrasound ray and allows calculation of the stacked signal along the beam (Figure 3c) as the sum of broadband (0.1–25 Hz) infrasound data recorded at the 4 array elements and shifted according to calculated propagation back azimuth. In this way, we strongly reduce the noise and enhance the waveform characteristics. Although the stacked waveform is obtained from the broadband infrasound record, spectral analysis of stacked waveforms clearly points out a narrow frequency component peaking between 2 and 3 Hz (Figure 3d).

Back azimuth *Baz* identifies the direction of infrasound propagation and in our case defines a vector pointing from the infrasound antenna towards the moving avalanche front. Considering the aperture of the array (≈60 m) and the frequency (up to 10 Hz) of recorded signal, we estimate an accuracy of ≈1° in back azimuth estimation. Back azimuth is marked by a constant decrease from 90°N to 75°N, before the trend changes and

a slight increase up to 82°N is observed (Figure 3b). Considering the topography between the glacier front and the array, the observed variation of the back azimuth is consistent with the ice mass flowing downhill within the gully to eventually turn anti-clockwise behind the Rotstock Ridge (Figure 3f).

The temporal changes of back azimuth can be used to obtain an estimate of the downhill velocity of the ice/snow mass. We assume the first detection, pointing at 90°N, to be consistent with the rupture time at the front of the glacier (Figure 3f). We assume the detection with the minimum back azimuth of 75°N, that is, reached 35 s after the onset, to reflect the timing when the collapsing ice mass hits the Rotstock Ridge, where the direction of the gully changes from North-Westward (≈290°N) to South-Westward (≈235°N). With this assumption, the avalanche travels a distance of ≈1 km between the front and the deflection point (Figure 1) in ca. 35 s. This reduces to ca. 33 s if the different propagation time of the infrasound wave from the moving source to the array is considered, with the ice mass approaching the array while flowing downhill. This corresponds to a mean velocity of ≈30 m/s. During this phase, recorded infrasound is characterized mostly by the high frequency component and by a smooth increase of pressure at all the sensors before the ice mass reaches the array. Our analysis thus confirms that the recorded high frequency signal, that is, highly coherent across the four array elements and tracked clearly with a variable back azimuth, is produced by the collapsed mass rapidly moving downhill.

In order to interpret the high-frequency (3 Hz) initial infrasonic signal generated as the ice avalanche approaches the antenna we approximate the avalanche volume as a moving sphere (Naugolnykh & Bedard, 1990). Its kinetic energy is partially transferred into infrasonic wave energy as the avalanche motion perturbs atmosphere pressure. The dominant frequency of the sound wave produced by the moving sphere scales with the inverse of its size (Landau & Lifshitz, 1959):

$$f = c / \pi D, \tag{1}$$

where c is the velocity of sound in the atmosphere while D is the diameter of the sphere. Despite being proposed more than 30 years ago already (Naugolnykh & Bedard, 1990) for the study of snow avalanches, Equation 1 has been applied only recently by Marchetti et al. (2020) to evaluate the size of a snow avalanche in Davos, Switzerland, and a careful experimental validation with a robust data set is still missing and still required. Nevertheless, given the nature of ice avalanches (Alean, 1985), and the abrupt change of bedrock gradient at Eiger glacier, the rigid sphere assumption might be acceptable.

For the May 29, 2017 collapse with a dominant infrasonic frequency of 2.85 Hz (Figures 3d and 3e) and an assumed sound propagation velocity of 330 m/s, Equation 1 predicts a moving sphere diameter D of 36.9 m corresponding to a sphere volume of 26,255 m^3. By considering an uncertainty of peak frequency estimation between 2.7 and 3 Hz (Figure 3e), estimated volume ranges between a minimum of 22.500 and a maximum of 30.900 m^3 ($35 < D < 38.9$). Such values are 2–3 times larger than the volumes estimated from radar images. A wrong estimate of sound propagation velocity ($325 < c < 335$ m/s), consistent with ambient temperature between −10°C and 5°C would affect the volume estimate for <5%.

6. Modeling the Low Frequency (0.1 Hz) Oscillation

The lack of coherence inhibits application of array techniques to the signal below 1 Hz (Figure 2b). We propose that the low frequency (0.1 Hz) pressure oscillations are a manifestation of air streaming around the moving avalanche mass. Approximating the avalanche mass again as a rigid sphere, the behavior of the fluid is controlled by the Reynolds number ($\Re$), defined as:

$$\Re = D v \rho / \mu, \tag{2}$$

where D is the diameter of the sphere, estimated above from the dominant >1Hz frequency to be 36.9 m, v is its velocity, assumed to be ≈30 m/s, and ρ and μ are the density and viscosity of air, that we assume here as 1.3 kg/m^3 and 1.7×10^{-5} $Pa \cdot s$ for an external temperature of 0°C. The corresponding $\Re$ is on the order of 10^7, thus satisfying the assumptions for an ideal fluid ($\mu \to 0, \Re \to \infty$).

The problem can be described as an inviscid flow, with no boundary layer and no viscous wake downstream the sphere. In this case, the air flow around the sphere is a potential flow, where the velocity field (**v**) is a
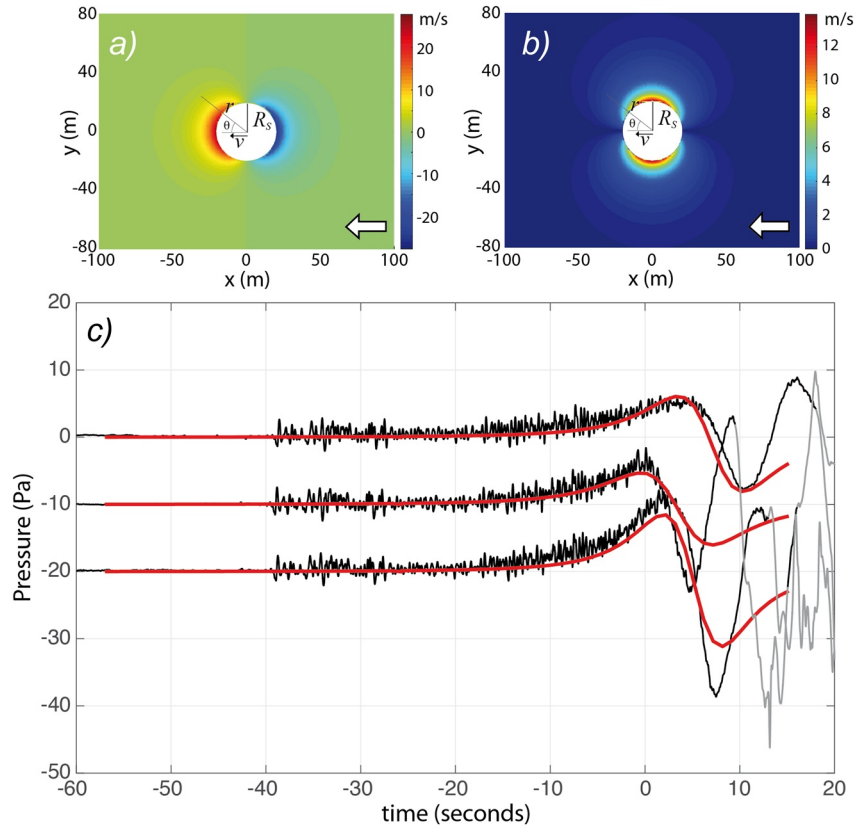
Figure 4. Radial v_r (a) and tangential v_θ (b) components of the inviscid flow induced by the moving sphere in surrounding air. The white arrow shows the sphere movement direction. Comparison (c) between the recorded infrasound pressure (black) and the modeled pressure at the array (red). Recorded waveforms are colored in gray after the spurious signal is recorded. Waveforms are aligned in time, according to the amplitude and timing of the positive peak of the second element of the array (mic 2). Comparison is limited to the first 3 elements of the array were at least the first positive peak of the low frequency oscillation is fully recorded.

laminar field with no vorticity and is fully described analytically by its radial (v_r) and tangential (v_θ) components (Landau & Lifshitz, 1959):

$$v_r = v\left(\frac{R_S^3}{r^3}\right)\cos\theta \tag{3}$$

$$v_\theta = v\left(\frac{R_S^3}{r^3}\right)\sin\theta \tag{4}$$

where v is the velocity of the sphere, R_S is the sphere radius, r is the radial coordinate, with $r = 0$ at the barycenter of the sphere, and θ represents the angular coordinate, for which $\theta = 0$ in the direction of the motion of the sphere. Both equations are defined only when $r > R_S$. Both radial (Equation 3) and tangential (Equation 4) velocity components $\to 0$ with increasing distance (r) from the sphere.

According to Equations (3 and 4), air molecules located along the trajectory of the sphere ($\theta = 0$) have only a radial velocity component, that is, positive in front of the sphere (i.e., air is pushed ahead by the sphere), while it is negative behind (i.e., air is pulled by the moving sphere). For all other positions, the air velocity field is characterized by both radial and tangential components, resulting in air flow streamlined around the sphere (Figure 4).

The velocity field **v** (Figures 4a and 4b), given by Equations 3 and 4, is characterized by a non-zero gradient ($\nabla \mathbf{v} \neq 0$), which means that the velocity is not constant around the sphere. Therefore, considering a unit volume V_o, identified by the closed surface S, at a given position nearby the sphere, influx air velocity will differ from efflux air velocity, thus resulting in $\Phi_S(\mathbf{v}) \neq 0$. This will produce, within the unit volume (V_o) a net air flux resulting in a change in the number of air moles (Δn) and thus, according to the ideal gas equation, in a change of pressure (ΔP):

$$\Delta P = \frac{\Delta n R T}{V_o},$$ (5)

where R is ideal gas constant and T is the absolute temperature, that are both assumed as constant. Considering that the ratio between the time evolution of the volumetric flux and the unit volume ($\frac{\Phi_S(\mathbf{v})s}{V_o}$) equals the ratio between the relative variation of the number of air moles ($\frac{\Delta n}{n}$), and by applying the divergence theorem, that relates the flux across a closed surface of the velocity field to the volumetric integral of $\nabla \cdot \mathbf{v}$:

$$\Phi(\mathbf{v}) = \int_V \nabla \cdot \mathbf{v} dV,$$ (6)

We can estimate the pressure variation ΔP induced by the moving sphere as:

$$\Delta P = \frac{P_o s}{V_o} \int_V \nabla \cdot \mathbf{v} dV,$$ (7)

where P_o is pressure in the unit volume for undisturbed conditions.

For each array element and following Equations 3–7, we calculate the pressure variation induced by the avalanche motion by assuming a sphere with radius spanning between 8 and 26 m, with a velocity spanning between 20 and 35 m/s and following six possible trajectories that are consistent with the measured back azimuth (Figure 3f). A total of 960 simulations were performed. The velocity is mostly affecting the frequency content of modeled waveform, with higher velocities resulting in higher frequencies, while radius and trajectory are mostly controlling the modeled pressure amplitude, with larger radius/shorter sphere-to-receiver distance leading to higher modeled pressure amplitude. An absolute minimum between recorded and modeled data is missing, thus preventing the possibility to fully invert the avalanche evolution without independent information on the trajectory and/or size, but still some general constraints are possible. Figure 4c shows the comparison of raw infrasound data and modeling for one of the best fits, obtained with a sphere radius of 20 m and a velocity of 27 m/s.

The timing of maximum amplitude of the low frequency (0.1 Hz) oscillation at different array elements coincides with the instant when the axis connecting the sphere's barycenter and the array element is at $\theta = 90°$ with respect to the sphere's moving direction (Figure 4c). At that point the radial velocity turns negative and the tangential velocity starts to decrease (Figure 4c) leading to a decrease of the modeled velocity flux. The model fails to reproduce the tail of the signal. This might result from the fact that the velocity field (**v**) described by the Equations 3 and 4 derived for inviscid flows typically fails to reproduce the velocity field behind the sphere, as it was experimentally observed that vortices develop and the flow decouples from the sphere (d'Alembert paradox [Landau & Lifshitz, 1959]).

7. Discussion and Conclusion

The infrasound array records of this major ice collapse ($\approx 10{,}000 \, \text{m}^3$) from the front of the hanging glacier on Mount Eiger, Switzerland, allowed to investigate the nature of infrasound energy radiation from a falling ice mass and to evaluate the potential of infrasound array analysis to monitor avalanching glaciers.

We confirmed that a glacier collapse is an efficient source of infrasound waves. Infrasound produced the falling ice mass is tracked by an array with a varying back azimuth that reflects, once combined with the local topography, the ice avalanche trajectory. Although a careful calibration with additional data will be required, we estimated the volume of the falling ice mass, in the assumption of a rigid sphere, to be 2–3 times larger than volume estimated from radar images. Such a discrepancy is possibly suggesting that the assumption of a rigid sphere is inappropriate and Equation 1 inadequate, or that the granular ice-snow

avalanche mass undergoes dilatation while flowing downhill. Indeed, significant dilatation of the ice-snow granular material may occur as it moves over non-erodible rough terrain (Dufresne, 2012) explaining a larger moving volume compared to the initially detaching volume. Nevertheless, these results highlight the potential of infrasound records to remotely estimate collapse trajectories and, once corroborated with additional studies, volumes.

The presented results show also that under certain conditions a broadband signal can be recorded, being induced by the air flux around the moving ice mass. Modeled infrasound is able to reproduce the amplitude, the duration, the timing and the different frequency content of the wave recorded at the different array elements, once a sphere with 20 m radius is considered traveling around 27 m/s. The comparison is limited to the first 3 elements of the array, where the low frequency oscillation is recorded properly. The positive peak is first recorded at sensor 2 and eventually at sensor 1, that is, furthest away along the trajectory. Misfits for the signal onset might be due to the wrong assumption on the dimension and velocity of the ice collapse, the trajectory as well as the assumption of the rigid sphere instead of a mass that is, likely breaking into pieces along the trajectory. Although the modeling results are not providing a unique solution, it points to a volume around 33,000 m^3, that is, >3 times the value obtained from radar, but in general agreement with the one inferred from the peak frequency of recorded infrasound (Equation 1). Again this discrepancy might derive from the strict assumptions or might suggest an increase of the avalanche volume along the trajectory for ice breaking into pieces. Moreover, it suggests a velocity of 27 m/s that is, in good agreement with the value (30 m/s) estimated from infrasound array analysis.

Our simple model explains the timing, the relative amplitude and the dispersive nature of the recorded low frequency (<0.1 Hz) infrasonic wavefield, and explains the broadband frequency characteristics of the recorded signal. Given the rapid decrease of the amplitude of the velocity field with distance from the source (Equations 3 and 4) such an effect is expected primarily for data recorded near the moving source.

Given the short computing time of infrasound array processing, with events possibly identified, and warning issued, within 2 min after their occurrence, and its efficiency to identify signals related to moving sources (Marchetti et al., 2015), this could be used as an additional system to radars and/or cameras to provide quantitative information, in near real-time, on ice avalanches, that might reflect the general stability on an hanging glacier front.

Data Availability Statement

Infrasound array data of the collapse are freely available at the OSF Open Science Framework repository (https://osf.io/ynjm2/).

References

Alean, J. (1985). Ice avalanches: Some empirical information about their formation and reach. *Journal of Glaciology*, *31*(109), 324–333. https://doi.org/10.3189/s0022143000006663

Allstadt, K. E., Matoza, R. S., Lockhart, A. B., Moran, S. C., Caplan-Auerbach, J., Haney, M. M., et al. (2018). Seismic and acoustic signatures of surficial mass movements at volcanoes. *Journal of Volcanology and Geothermal Research*, *364*, 76–106. https://doi.org/10.1016/j.jvolgeores.2018.09.007

Dalban Canassy, P., Faillettaz, J., Walter, F., & Huss, M. (2012). Seismic activity and surface motion of a steep temperate glacier: A study on Triftgletscher, Switzerland. *Journal of Glaciology*, *58*(209), 513–528. https://doi.org/10.3189/2012JoG11J104

Dalban Canassy, P., Walter, F., Husen, S., Maurer, H., Faillettaz, J., & Farinotti, D. (2013). Investigating the dynamics of an alpine glacier using probabilistic icequake locations. *Journal of Geophysical Research: Earth Surface*, *118*, 2003–2018. https://doi.org/10.1002/jgrf2009710.1002/jgrf.20097

Dufresne, A. (2012). Granular flow experiments on the interaction with stationary runout path materials and comparison to rock avalanche events. *Earth Surface Processes and Landforms*, *37*(14), 1527–1541. https://doi.org/10.1002/esp.3296

Faillettaz, J., Funk, M., & Sornette, D. (2011). Icequakes coupled with surface displacements for predicting glacier break-off. *Journal of Glaciology*, *57*(203), 453–460. https://doi.org/10.3189/002214311796905668

Faillettaz, J., Funk, M., & Vincent, C. (2015). Avalanching glacier instabilities: Review on processes and early warning perspectives. *Reviews of Geophysics*, *53*, 203–224. https://doi.org/10.1002/2014RG000466

Faillettaz, J., Sornette, D., & Funk, M. (2011). Numerical modeling of a gravity-driven instability of a cold hanging glacier: Reanalysis of the 1895 break-off of Altelsgletscher, Switzerland. *Journal of Glaciology*, *57*(205), 817–831. https://doi.org/10.3189/002214311798043852

Field, C. B., Barros, V. R., Mach, K. J., Mastrandrea, M. D., van Aalst, R. A., Adger, W. N., et al. (2014). Technical summary. In *Climate change 2014: Impacts, adaptation, and vulnerability. Part A: Global and sectoral aspects. Contribution of working group II to the fifth assessment report of the Intergovernmental panel on climate change* (pp. 35–94). Cambridge, United Kingdom and New York, NY, USA: Cambridge University Press.

Johnson, J. B., & Ronan, T. J. (2015). Infrasound from volcanic rockfalls. *Journal of Geophysical Research: Solid Earth*, *120*, 8223–8239. https://doi.org/10.1002/2015JB012436

Kääb, A., Leinss, S., Gilbert, A., Bühler, Y., Gascoin, S., Evans, S. G., et al. (2018). Massive collapse of two glaciers in western Tibet in 2016 after surge-like instability. *Nature Geoscience*, *11*(2), 114–120. https://doi.org/10.1038/s41561-017-0039-7

Landau, L. D., & Lifshitz, E. M. (1959). *Fluid mechanics*. Pergamon Press.

Marchetti, E., Ripepe, M., Ulivieri, G., & Kogelnig, A. (2015). Infrasound array criteria for automatic detection and front velocity estimation of snow avalanches: Towards a real-time early-warning system. *Natural Hazards and Earth System Sciences*, *15*, 2545–2555. https://doi.org/10.5194/nhess-15-2545-2015

Marchetti, E., van Herwijnen, A., Christen, M., Silengo, M. C., & Barfucci, G. (2020). Seismo-acoustic energy partitioning of a powder snow avalanche. *Earth Surface Dynamics*, *8*, 399–411. https://doi.org/10.5194/esurf-8-399-2020

Marchetti, E., Walter, F., Barfucci, G., Genco, R., Wenner, M., Ripepe, M., et al. (2019). Infrasound array analysis of debris flow activity and implication for early warning. *Journal of Geophysical Research: Earth Surface*, *124*, 567–587. https://doi.org/10.1029/2018JF004785

Margreth, S., Funk, M., Tobler, D., Dalban, P., Meier, L., & Lauper, J. (2017). Analysis of the hazard caused by ice avalanches from the hanging glacier on the Eiger West face. *Cold Regions Science and Technology*, *144*, 63–72. https://doi.org/10.1016/j.coldregions.2017.05.012

Meier, L., Jacquemart, M., Blattmann, B., Wyssen, S., Arnold, B., & Funk, M. (2016). Radar-based warning and alarm systems for alpine mass movements. In *Proceedings of INTRAPRAEVENT 2016, 30 May-2 June* (pp. 960–968). Lucerne, Switzerland.

Naugolnykh, K., & Bedard, A. (1990). Model of the avalanche infrasound radiation. In *Proceeding of international snow science workshop, Jackson, WY, 19-24 September 2004* (pp. 871–872).

Pralong, A., & Funk, M. (2006). On the instability of avalanching glaciers. *Journal of Glaciology*, *52*(176), 31–48. https://doi.org/10.3189/172756506781828980

Pralong, A., Funk, M., & Lüthi, M. P. (2003). A description of crevasse formation using continuum damage mechanics. *Annals of Glaciology*, *37*, 77–82. https://doi.org/10.3189/172756403781816077

Preiswerk, L. E., Walter, F., Anandakrishnan, S., Barfucci, G., Beutel, J., Burkett, P. G., et al. (2016). Monitoring unstable parts in the ice-covered Weissmies northwest face. In *13th congress interpraevent 2016*.

Raymond, M., Wegmann, M., & Funk, M. (2016). *Inventar gefährlicher gletscher*. VAW/ETH Report (p. 182).

Schimmel, A., Hübl, J., McArdell, B. W., & Walter, F. (2018). Automatic identification of alpine mass movements by a combination of seismic and infrasound sensors. *Sensors*, *18*(5), 1658. https://doi.org/10.3390/s18051658

Ulivieri, G., Marchetti, E., Ripepe, M., Chiambretti, I., De Rosa, G., & Segor, V. (2011). Monitoring snow avalanches in Northwestern Italian Alps using an infrasound array. *Cold Regions Science and Technology*, *69*, 177–183. https://doi.org/10.1916/j.coldregions.2011.09.006